PROCESS MODELING FOR FLUID-INTERFACE SUPPORTED RESIN PRINTING

S. Appana*, S. M. Ross*, C. Sims*, R. Schwerzel, A. S. Jariwala*

*George W. Woodruff School of Mechanical Engineering, Georgia Institute of Technology, Atlanta, GA 30318

Abstract

The article details the latest design and implementation of a stereolithography (SLA) based technique, Fluid Interface Supported Printing (FISP). The FISP technique involves printing from a thin resin layer above a static, immiscible support fluid. The support fluid prevents deflection of overhanging geometry by providing a buoyant force equal to that of the gravitational force due to the minute density difference between the support fluid and cured resin. Complex curing and shrinkage dynamics are a primary knowledge gap. A COMSOL multiphysics simulation model was developed to simulate the curing process, including volumetric light intensity and optimized parameters for chemical reaction kinetics. The article presents a pathway for further enhancing and validating the simulation model.

Introduction

Stereolithography (SLA) is the most common resin 3D printing process, popular for its ability to produce high-resolution, isotropic, and watertight products. The micrometer-scale layer thickness produces fine features with a smooth finish, ideal for prototyping intricate geometries and unique concept models. The layer-by-layer printing process uses photocuring to convert liquid resin, or a fluid prepolymer, into a hardened polymer under the presence of ultraviolet (UV) or visible light. Photocuring enables high temporal and spatial control within a fraction of a second. Modern SLA printers have a vat to contain liquid resin, a UV light source emitting light at the designated wavelength, a resin-resistant film between the resin and the light source, and a build plate to hold the part and control layer-based curing. The UV light source projects UV light onto the resin's surface in the desired shape by using a digital light processing (DLP) system or by implementing an LCD mask. Controlling a two-dimensional light projection allows the printer to cure an entire layer with one projection accurately. Light exposure time and intensity control the layer thickness.

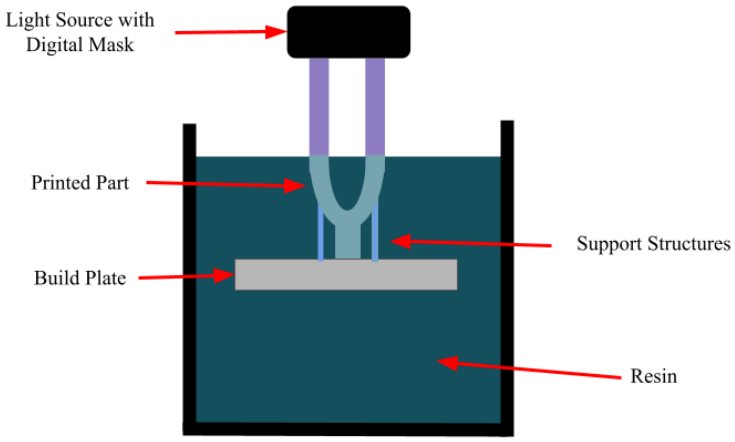

Figure 1: Typical Top-Down Stereolithography Printing Diagram

This paper focuses on a top-down printing approach where the light source is above the resin and projects light downward onto the resin. Fig. 1 shows a diagram of a typical top-down SLA printer. This approach is necessary to accommodate the fluid-interface supported printing (FISP) process, as explained in elaborate detail by Mulka [1]. Fig. 2 shows a diagram of the FISP system. The FISP system integrates a fluid support system, or saline solution, with a density equivalent to solid, cured resin [1]. Given that the density of cured resin is greater than the liquid resin, the resin will remain afloat on top of the support fluid. The FISP printing system enables printing without solid, sacrificial support structures [1]. Support structures increase surface deformation, post-processing time, and wasted photosensitive resin.

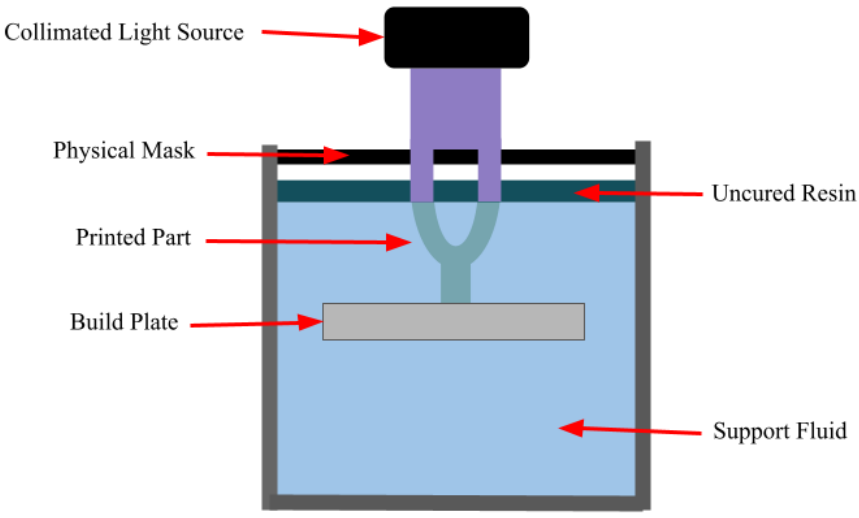

Figure 2: FISP Diagram

A principal difficulty with the top-down printing approach is that the printer must combat inhibition by molecular oxygen during polymerization. Molecular oxygen in the resin during curing results in an incomplete cure, represented by a tacky surface or a failure to cure [2]. Two

mechanisms exist for combatting oxygen-inhibition: removing/limiting oxygen from the curing area or modifying the resin's formulation for greater insensitivity [2]. Commercial printers and resins use oxygen-sensitive, acrylate-based resins due to their efficient wetting and speedier printing. Therefore, commercial printers restrict oxygen from entering the curing environment through various mechanisms. Two of these mechanisms include using an alternate-gas pumping system to displace oxygen or implementing a fluorinated ethylene propylene (FEP) film to create a "dead zone" that better controls curing. Displacing oxygen adds a layer of control complexity to the system, whereas the films retain a significant separation force between the cured part and the film. Separation forces are the forces that the part incurs when the build plate's height is adjusted to print the next layer. Fig. 3, taken from a film separation analysis conducted at Xi'an University of Technology, compares the separation force between two FEP films with varying flexibility. This analysis shows that the FEP film separation force is non-negligible.

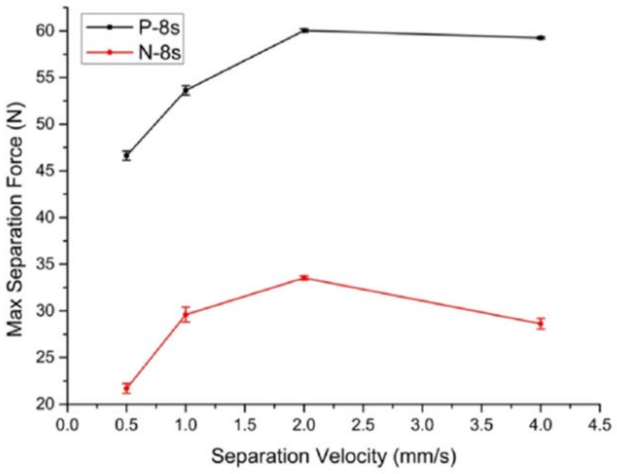

Figure 3: Separation forces for FEP film-based printing systems [3]

Fig. 4 demonstrates overhanging samples printed without supports on a commercial bottom-up stereolithography 3D printer that implements an FEP film. Evidently, the stiction force to the FEP film is non-negligible, resulting in deformities.

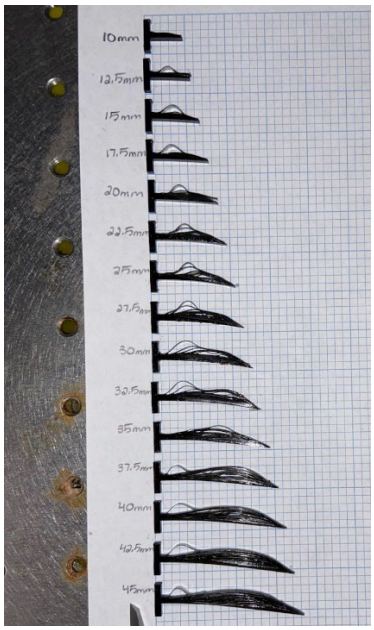

Figure 4: Supportless cantilevers printed from a commercial SLA printer (AnyCubic Photon M3) showing the sticking of top layers with the FEP film and drooping of overhang features

The present FISP system aims to polymerize resin in a top-down fashion where the resin is directly exposed to air, as opposed to using a film. Fig. 5 presents that film separation forces result from adhesion forces and Stefan forces [4]. To eliminate separation forces, the system removes the film-resin interface by curing the resin directly to the open-air.

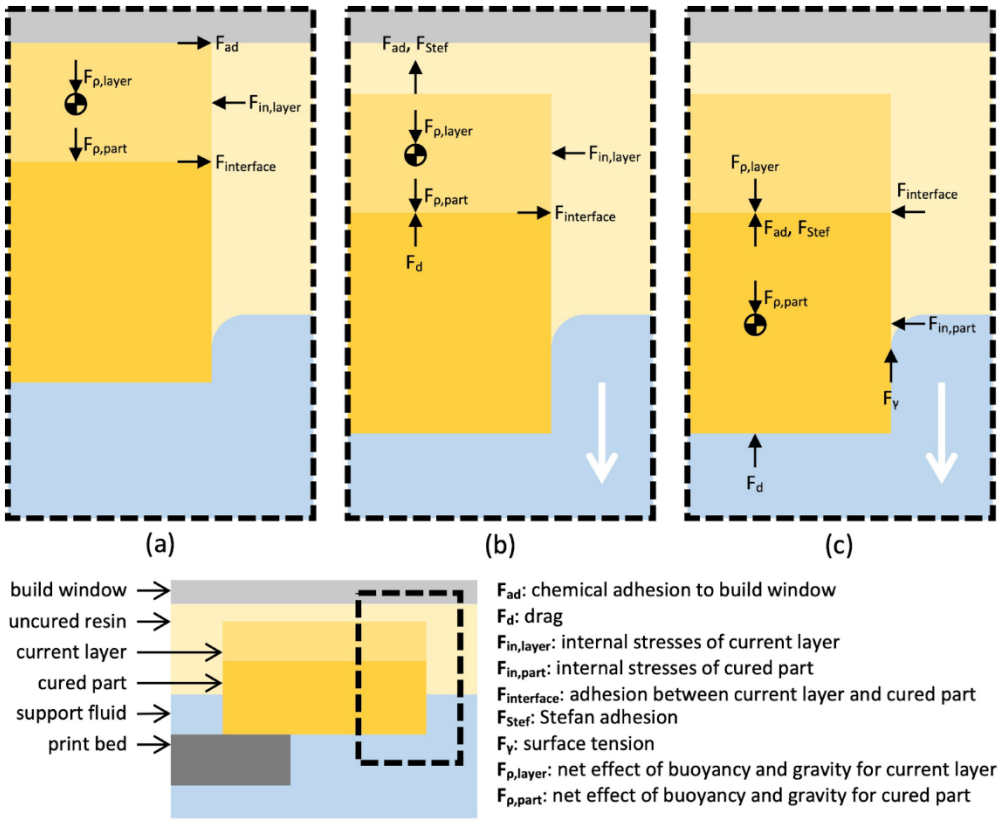

Figure 5: Separation Force Free Body Diagram [4]

A complexity of curing with an air-resin boundary is the potential increase in oxygen inhibition resulting from the resin's increased exposure to oxygen. Moreover, the FISP system presents two oxygen flux boundaries: atmospheric oxygen from the top, and dissolved oxygen in the saline from the bottom. Oxygen inhibition may be counteracted by increasing the concentration of free radicals to increase the likelihood of initiating polymerization. More free radicals can be generated by increasing the light's intensity incident on the resin, which also results in quicker polymerization. Given the oxygen boundaries, the paper focuses on the effect of oxygen on resin curing while assuming the part deformation is negligible.

The reaction and resin curing is analyzed using the Multiphysics modeling/simulation tool COMSOL. Previously, Emami and Rosen [5] updated a COMSOL model that described the photopolymerization reactions by incorporating the light field effect, photobleaching, oxygen inhibition, and volumetric intensity. The primary output of the model is the cure height for a given exposure, and this is given in terms of the degree of cure (DoC). While this model formed the basis for the present COMSOL model, parameters of the resin, such as molecular weight, density, and photoinitiator percentage, had to be updated to match the current commercial resin. Although many parameters could be gathered from relevant literature and manufacturer specifications, experimental data was collected to determine appropriate values for the propagation and termination rate constants. Additionally, boundary flux conditions, which were not included previously, are necessary to represent the current experimental setup accurately.

While the main goal of this research is to develop a working FISP system, the COMSOL model aids this goal by providing a theoretical model which can be used to predict and explain observed and new curing geometries. Without a model to support experimental results, it would be difficult to predict how the FISP system would behave, or whether observed results are consistent with the general model. The COMSOL model helps fill in these gaps and aid in developing the FISP system. The model developed will be a valuable resource when simulating parameter variations and grayscale patterns.

Methods

The AnyCubic™ 405 nm clear resin was selected for its low viscosity, nonpolar composition, and lack of dyes. Given the configuration of FISP, the resin must rapidly spread across the surface of the support fluid and remain immiscible with water to develop a boundary layer. The AnyCubic™ 405nm liquid resin consists of a density close to water at 1.12 g/mL, and the cured part consists of a density close to 1.184 g/mL [6]. The density range of the resin lies within the density range for undersaturated or saturated saltwater solutions.

Using a commercial resin allows for repeatability, but a few variables are not readily available for modeling the resin. An experimentally determined working curve was developed for the resin to determine the values of the unknown variables. The working curve was also used to compare the AnyCubic Clear resin's behavior when the light intensity is varied and when the resin is atop a support fluid. The variation in light intensity allows for comparison between the resin's reaction when supplied with similar energy inputs at different rates. The second parameter accounts for potential oxygen inhibition due to dissolved oxygen in the support fluid. No materials were reused to obtain values to account for any degradation in the resin produced over multiple trials. The vat used for experimental data collection is a small souffle cup that contains a 3D printed part, saline support fluid, and AnyCubic Clear Resin. The 3D printed part adheres to the flood-cured part to prevent the part from floating away.

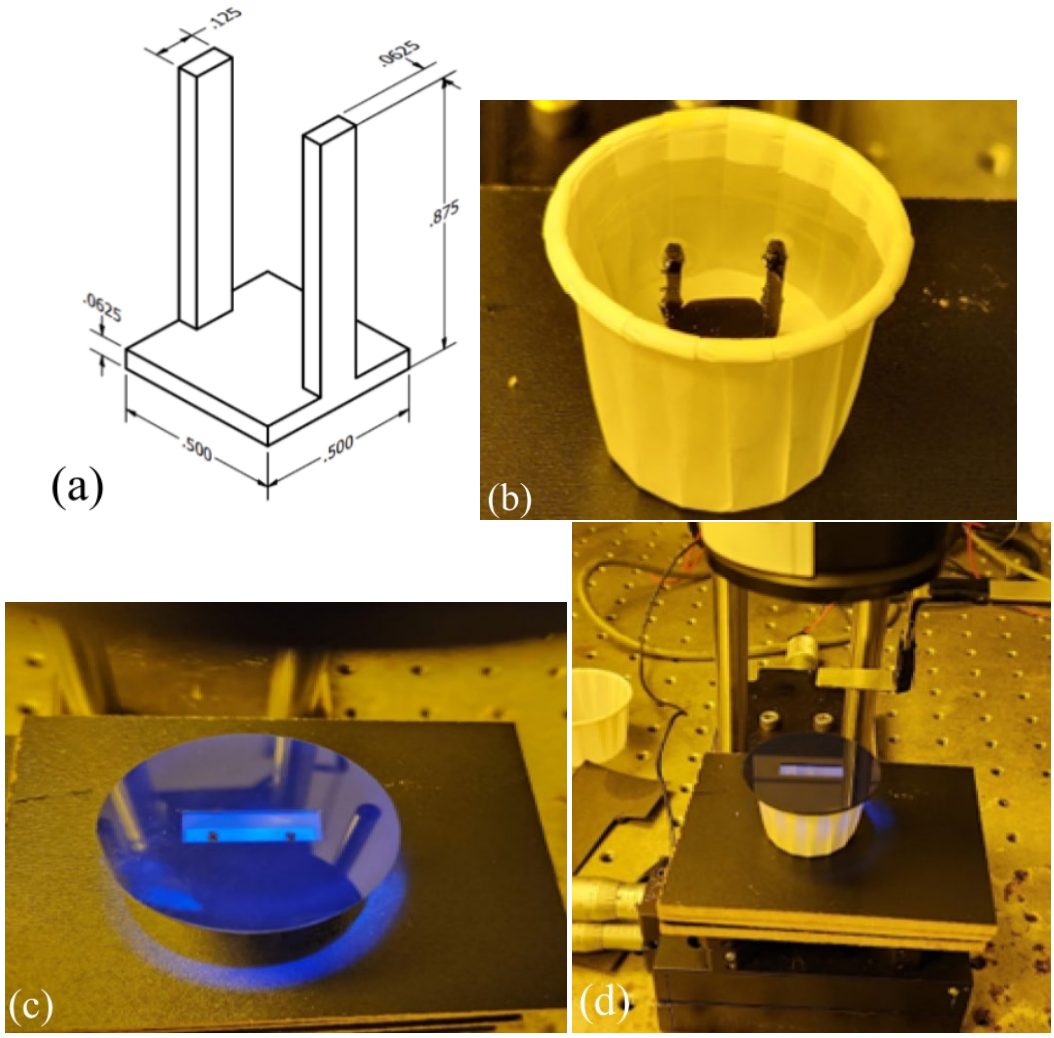

Figure 6: (a) 3D Printed Part Holder, (b) Souffle cup vat containing a 3D printed part submerged in saline support fluid and AnyCubic 405 nm clear resin, (c) profile of physical mask, (d) Photo of FISP experimental system

The desired height of the resin afloat on the support fluid was determined to be 7.5 mm to enable flood curing. The cup's primary dimensions and linear interpolation resulted in 8.777 mL of saltwater solution being deposited in the cup. However, the closest value of glassware gradation was 8.5 mL. Therefore, to maintain consistency between trials, 8.5 mL was deposited. The increase in distance from the light source caused by depositing 8.5 mL rather than 8.777 mL is negligible. Based on fundamental density-concentration calculations for saltwater, 24.749% weight of salt is necessary to achieve the desired density, 1.184 g/mL. The mask to produce a 0.75-inch by 0.25-inch rectangle, accounting for the light's divergence, was laser-cut using 0.1-inch-thick black acrylic.

The AnyCubic 405 nm clear resin contains the photoinitiator Ciba Irgacure 819. Figure 7 shows the ultraviolet light functional range of Irgacure 819. Although the commercial resin is advertised for 405 nm wavelengths of light, the wide variety of usable wavelengths for the

photoinitiator and the higher functionality to lower wavelengths motivated the use of a 365 nm Thorlabs light source.

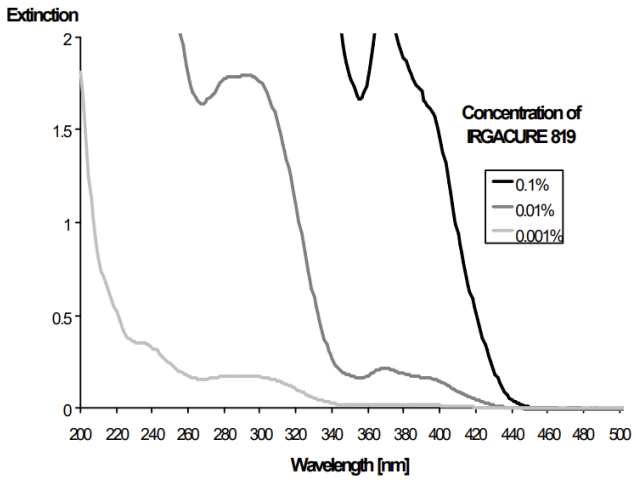

Figure 7: Functional range of Ciba Irgacure 819 at different concentrations

The parts were cured with a baseline light intensity of 1.6 mW/cm^2 of 365 nm light to provide a sufficient intensity to cure resin and overcome oxygen inhibition. To analyze the effect of curing resin at higher intensities, a trial consisted of curing with 4.8 mW/cm^2 light intensity. The control group was developed with no support fluid and an identical setup using 1.6 mW/cm^2 light intensity. The only post-curing operation performed was the wash with 95% IPA to remove excess resin cohering to the part following removal from the vat. Three measurements were taken along each part.

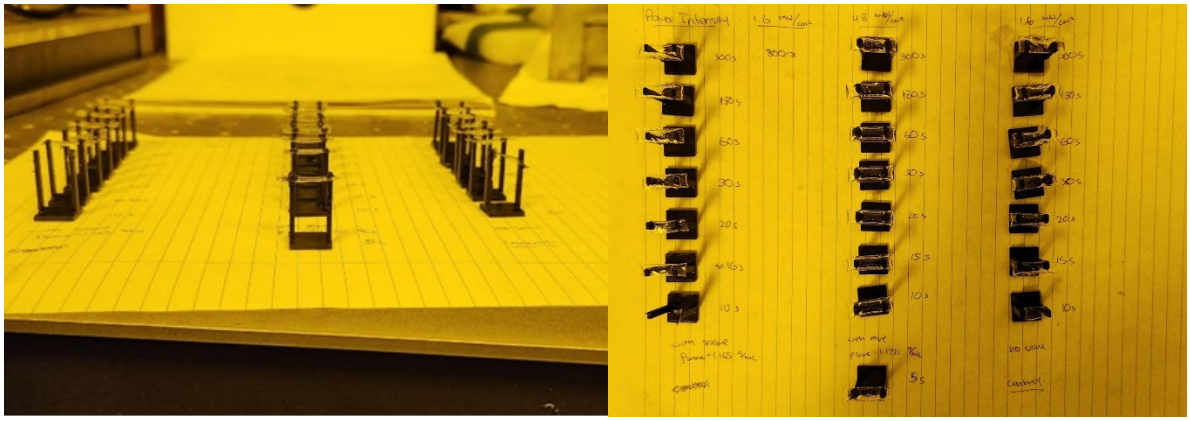

Figure 8: Parts produced from varying light intensity and support fluid

The parts were each measured using a micrometer with a miniscule torque limit to prevent significant deformations larger than ten microns when measuring thicknesses of parts.

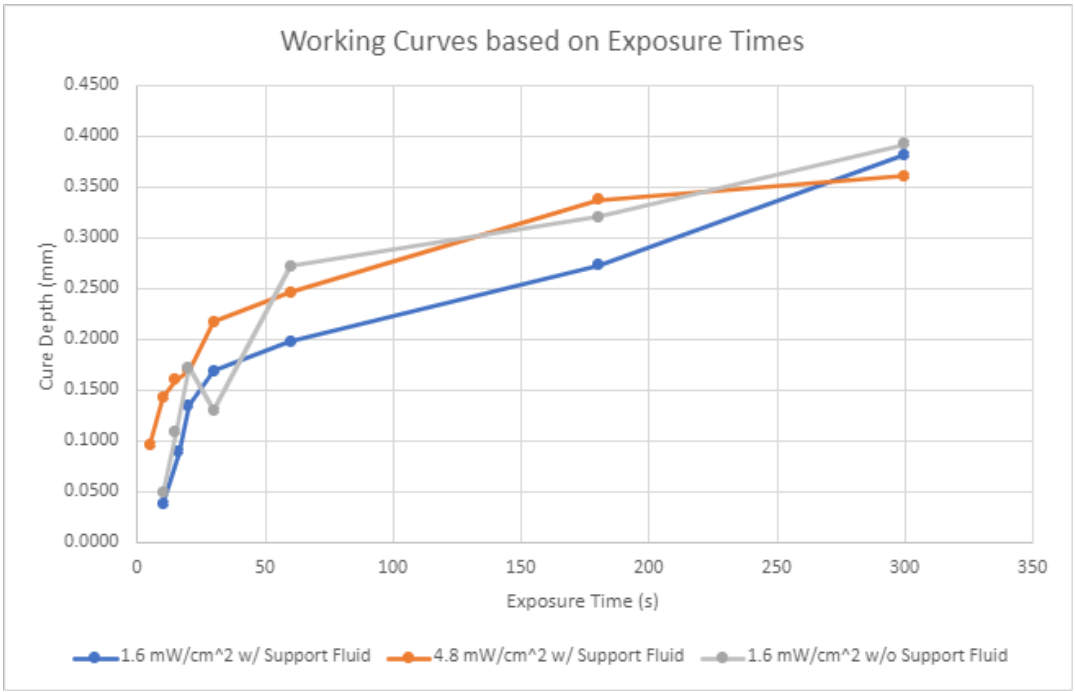

Figure 9: Working curve for the resin with respect to exposure time in seconds

Comparing the curves for parts cured using 1.6 mW/cm^2 with and without support fluid in Fig. 9 indicate that the support fluid had slowed down the rate of polymerization. This means that more energy was supplied to the system to cure parts of identical heights using a support fluid. Evidently, the FISP computational model must reflect these oxygen flux boundary conditions. There does appear to be one part defect which results in a lower cure depth than expected, which is likely an experimental error. Looking at the general shape of the curve, the results demonstrate a logarithmic trend as expected. The experiment can be further validated on the logarithmic scale for the x-axis.

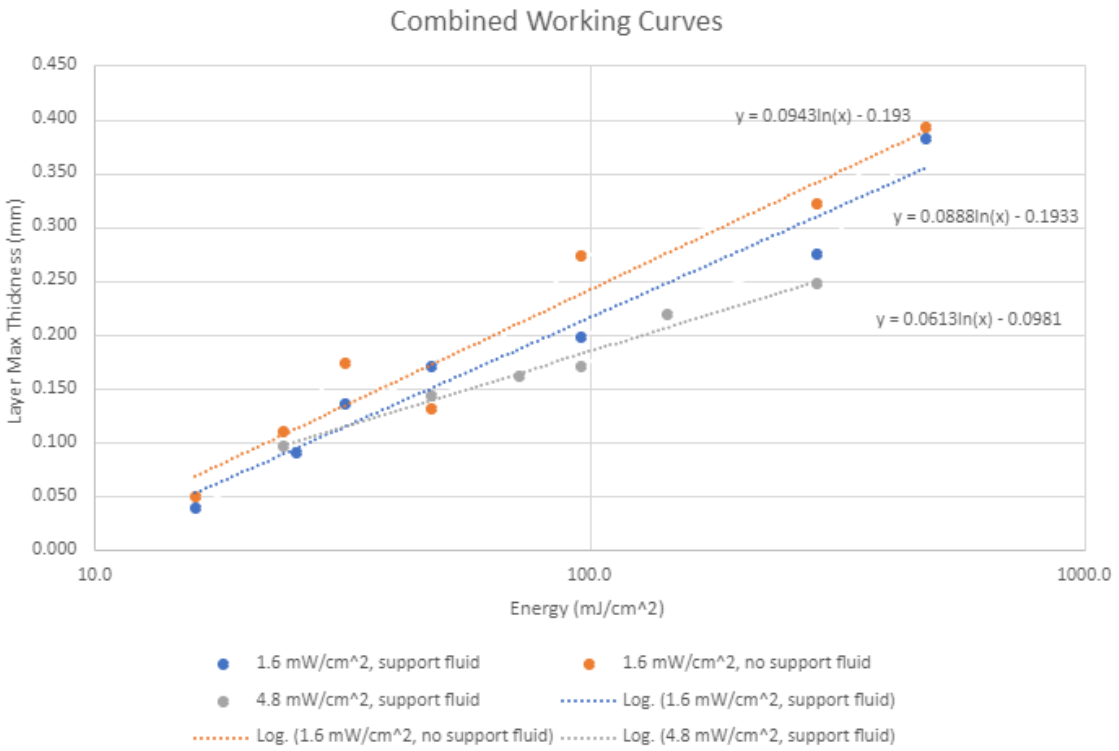

Figure 10: The data collected for the working curves are plotted on a logarithmic scale to observe the linear trend.

On the logarithmic scale, each of the datasets should contain a linear trendline. Using the trendlines computed by Excel's linear regression algorithms, the y-intercepts are negative, which is an indication that the data is valid since the activation energy is positive. In other words, a positive amount of energy must be introduced into the resin to initiate curing. For the COMSOL model parameter fitting, the logarithmic scale for exposure will allow for solution comparison.

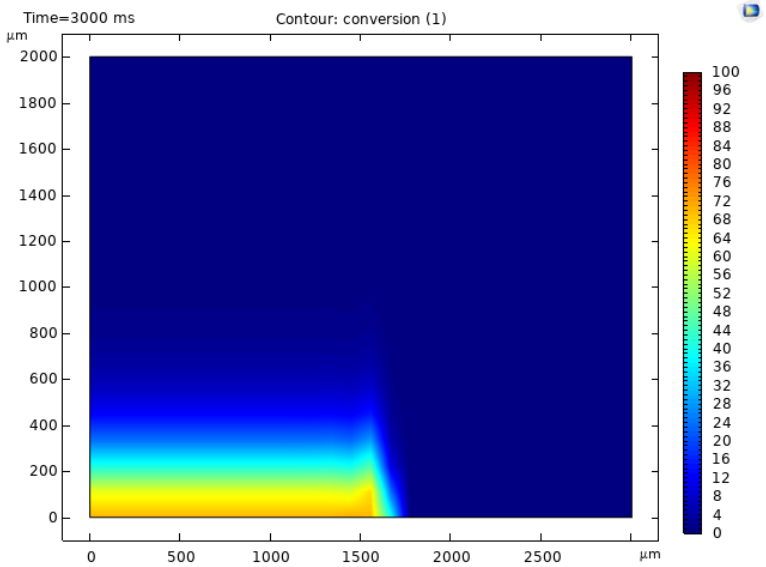

Figure 11: Two-dimensional Degree of Conversion (DoC) output of COMSOL model. A DoC of 20% was defined as fully cured on a gradient color scale from 0 – 100%. The axis of symmetry is on the left side of the resin field.

The COMSOL model is set up as a rectangular slice of a vat of uncured resin, with an axis of symmetry that creates a cylindrical curved geometry. Figure 11 shows the main output of the model, which is a two-dimensional plot of the resin's degree of conversion. Table 1 defines the properties of the resin, which are taken from the resin manufacturer [6], relevant papers, and Emami and Rosen's updated model [5]. The reaction equations, along with volumetric intensity and oxygen inhibition, are defined as described above. The photobleaching effect was ignored in the model.

Table 1: COMSOL Resin Parameters

Parameter	Variable Name	Units	Emami	Current
Initial concentration of O2 in resin	c_O2_0	mol/m^3	1.05	0.9
Quantum yield	Phi	-	0.6	0.95
Molar absorptivity	ep0	m^2/mol	14	75
Molecular weight of monomers	MW_monomer	kg/mol	0.296	0.27836
Molecular weight of initiator	MW	kg/mol	0.256	0.3404
Weight % of photoinitiator	wt	-	2	5
Density of monomers	Density_Monomer	kg/m^3	1110	953.67
Oxygen diffusion rate	DO2	m^2/s	1e-10	1e-10

The parameters changed in the current model involved decreasing the initial concentration in the resin from 1.05 to 0.9 based on a paper describing oxygen solubility in diacrylates [7]. The quantum yield was changed from 0.6 to 0.95 based on a recent paper on phenyl bis (2,4,6-trimethylbenzoyl)-phosphine oxide (BAPO) kinetics [8]. However, after these experiments were performed, a re-evaluation of several papers [9, 10] suggests that 0.6 was more accurate and will be changed in future research. The molar absorptivity was updated to 75 based on [11], which describes how much light is required to dissociate the photoinitiator into free radicals and how far the light can penetrate the resin. This substantial change is due to the type of photoinitiator used in the current resin (BAPO) compared to that in the previous resin (TPO). The oxygen diffusion rate was kept the same. The other parameters (molecular weight, density, and photoinitiator concentration) were calculated from the manufacturer's specifications [6]. After adjusting the parameters to represent the new resin better, sensitivity analysis was performed on the model to see the model's behavior in response to changing these different parameters, such as the molar absorptivity, quantum yield, and rate constants. This was done to ensure the model accurately represented photopolymerization, examine how these parameters affected the cure height and working curve, and form a basis for future optimization of the rate constants.

Results and Discussion

The primary analysis involved creating a working curve from the cured heights and exposure values and comparing the curve to the experimental working curve. When plotted on a logarithmic scale, the slope and intercept of each curve are unique to each run. For the model to match the experimental data, the slope and intercepts must match. However, the interest in this

study was how the different parameters affected the working curve, which can be seen in the plots below. An initial test was to determine whether the model responded adequately to changes in otherwise constant parameters, such as quantum yield. Figure 12 shows that the cure depth decreases as the quantum yield decreases and vice versa. This matches our expectations and follows from the quantum yield describing how many free radicals crosslink with monomers for each photon absorbed.

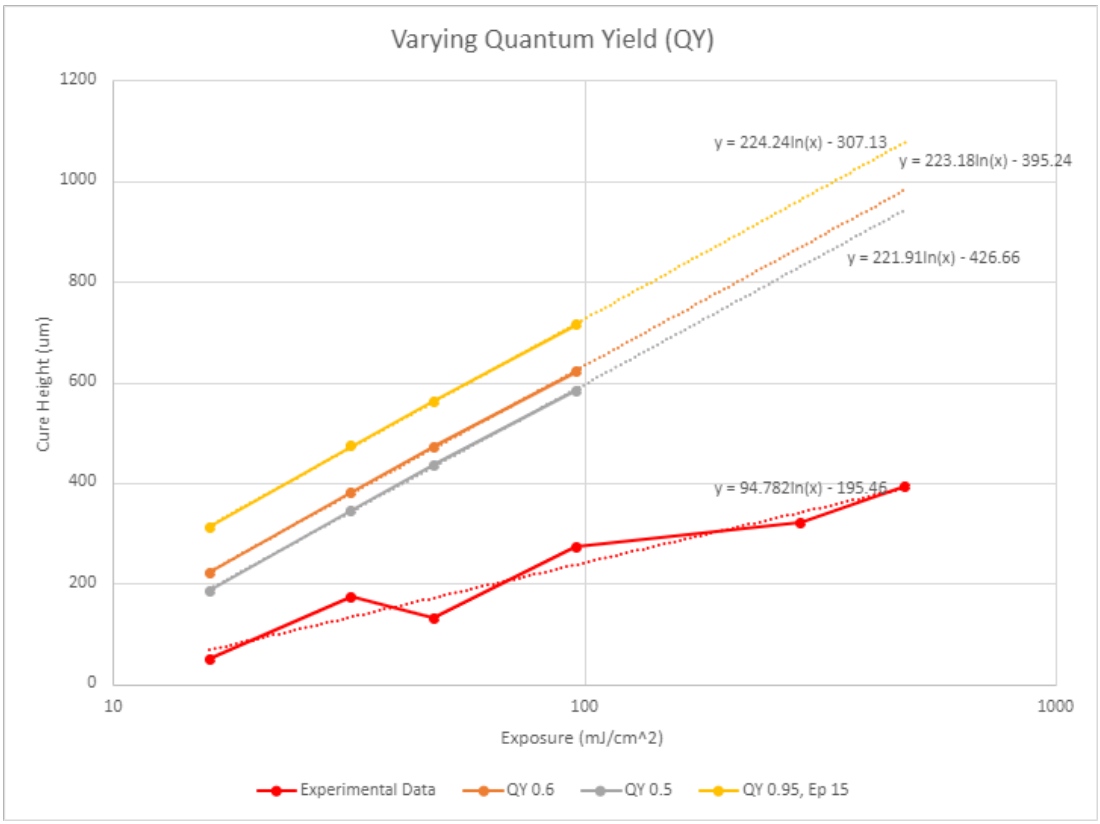

Figure 12: Working curves with varying quantum yield. As the quantum yield increases, the cure height increases with a nearly constant working curve slope.

Since the molar absorptivity has been adjusted significantly for the new resin, testing the behavior of the model in response to changing this parameter is important. Similar to the quantum yield, the molar absorptivity also shifts the working curve vertically, although it also changes the slope of the cure. Figure 13 shows that as the molar absorptivity decreases, the light can penetrate deeper into the resin since not as much is absorbed or needed by the shallower photoinitiator. This leads to a higher overall cure throughout the resin, but more cure especially deeper inside the resin. As the molar absorptivity increases, more light is needed to cure the resin, resulting in a lower cure throughout the resin. However, according to Beer Lambert's law, the intensity of light decreases with depth in the resin, thus reducing the cure further in the resin.

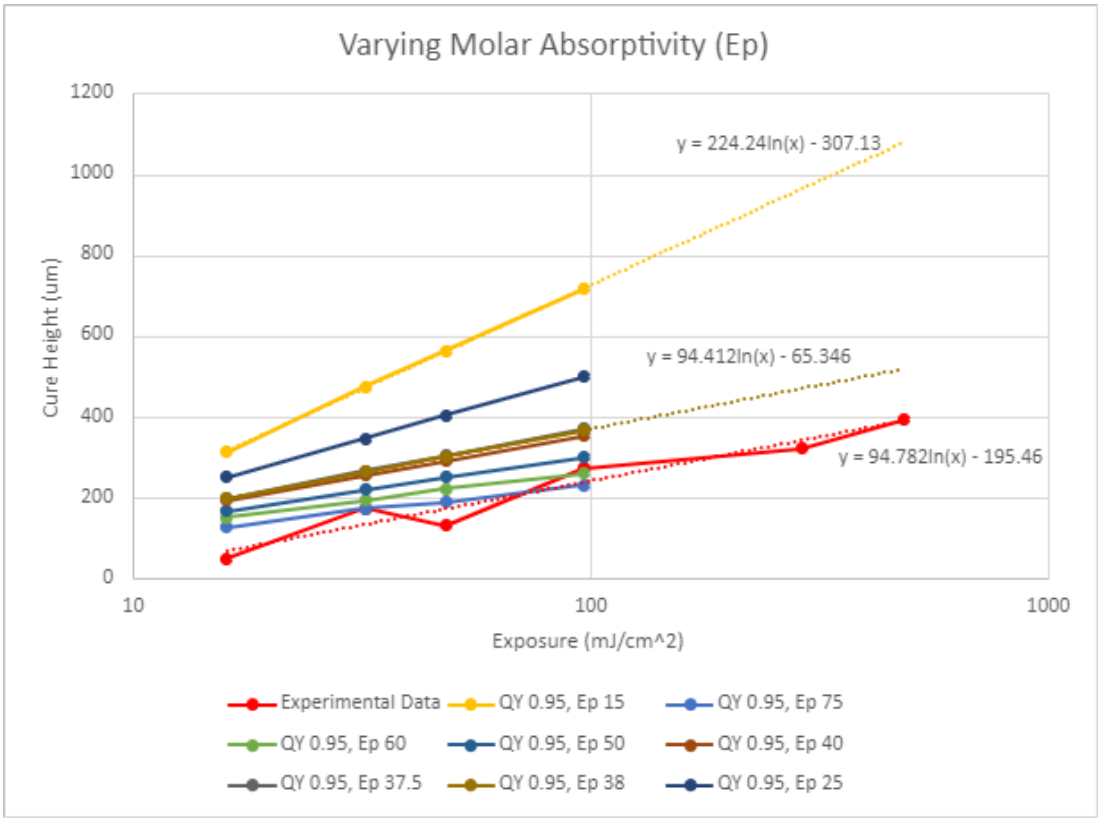

Figure 13: Working curves varying molar absorptivity. As the molar absorptivity increases, the cure height decreases with a decreasing working curve slope. This decrease is more significant deeper in the resin.

The primary focus of this analysis was the propagation and termination rate constants since these will be optimized to fit the experimental data after the parameters are set and the flux conditions added. The behavior of the rate constants can be seen below. As the propagation rate constant increases in Figure 14, the cure increases throughout the resin, and the working curve becomes more flat, indicating less dependence on exposure time. Conversely, cure increases with a decreasing termination rate constant in Figure 15, since the termination rate stops the crosslinking reactions. This analysis determines the parameters' effect on the cure height and working curve, which will be crucial in optimizing the model to fit the experimental data after the model is updated to include boundary fluxes and accurate resin parameters.

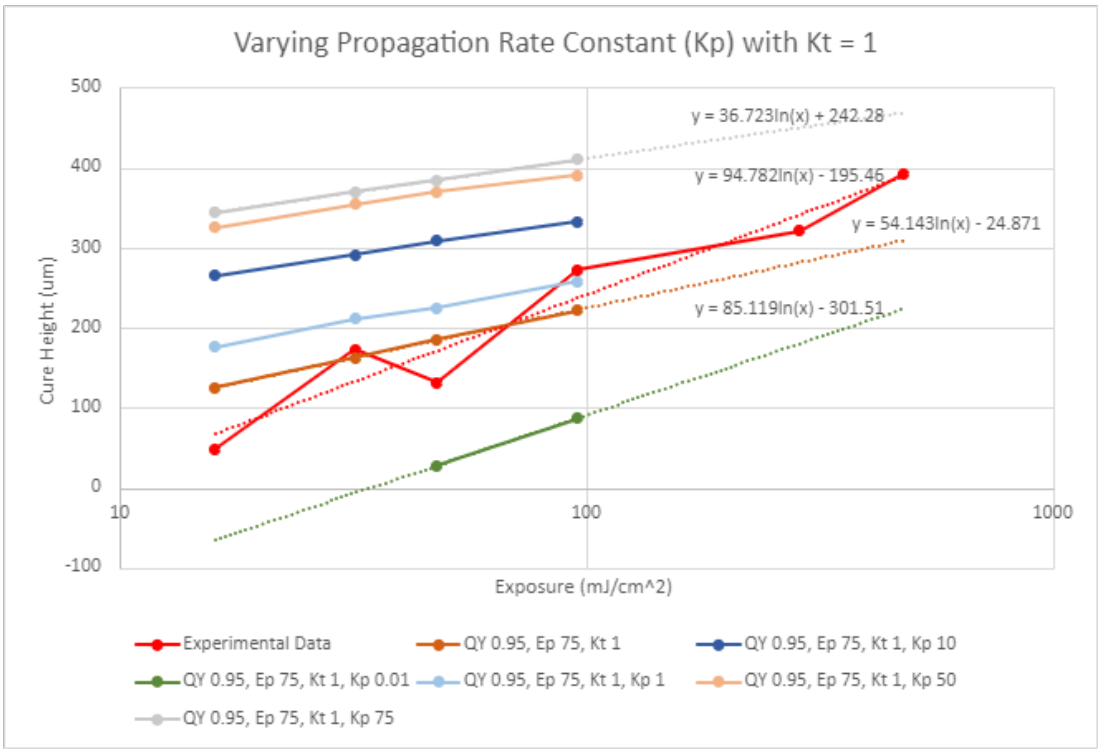

Figure 14: Working curves with varying propagation rate constant. As the propagation rate constant increases from 0.01 to 75, the cure height increases, although the working curve slope decreases.

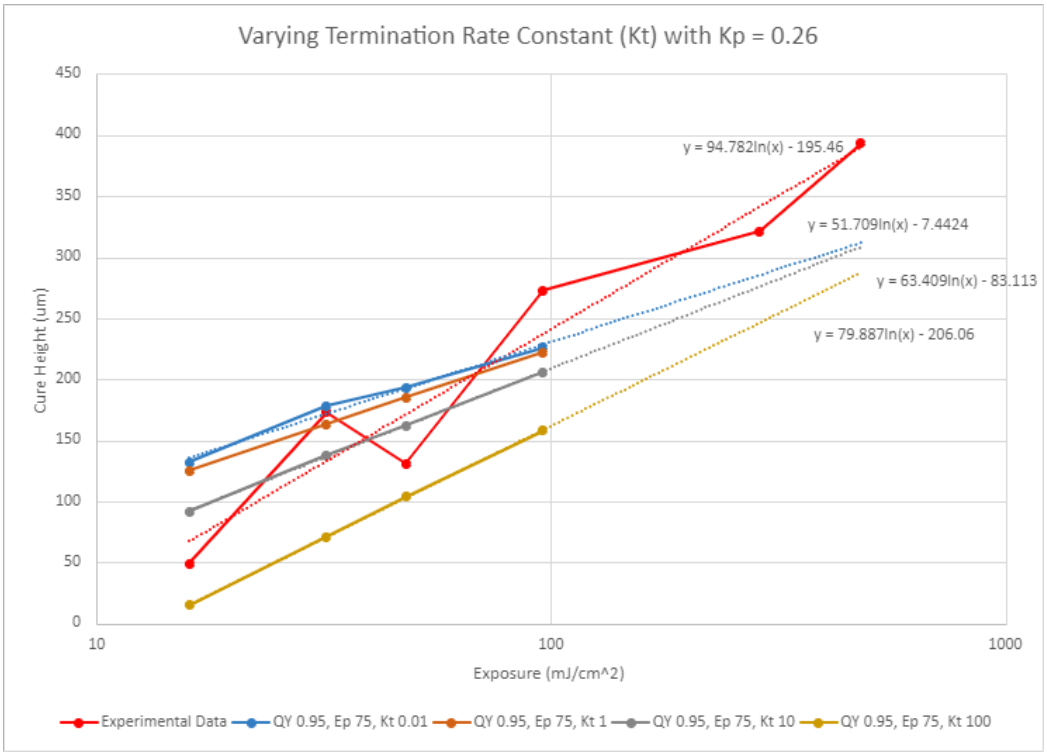

Figure 15: Working curves with varying termination rate constant. As the termination increases from 0.01 to 100, the cure height decreases, and the slope of the working curve increases.

Conclusion and Future Work

Several essential steps toward advancing the FISP system have been accomplished. Replacing the custom resin with a commercial resin has been successful and repeatable in the experimental curing phase. Through experimentation, research, and simulation, several of the essential resin parameters for the COMSOL model have been adjusted and tested. The COMSOL model has been updated to include the commercial resin's new molecular weights, densities, and photoinitiator percentages. The quantum yield and molar absorptivity have also been updated based on research on BAPO photoiniators. The experimental working curve data provides a basis for future optimization of the propagation and termination rate constants for the COMSOL model. While the experimental and the simulated working curves still disagree regarding slope and initiation energy (y-intercept), they are within the same order of magnitude. This demonstrates that the current model approximates our experimental photopolymerization but requires further parameter optimization.

The possibility of open-air curing has also been confirmed through experimentation. Previously, there were concerns about oxygen inhibition preventing curing. However, experimentation has proven that open-air curing is feasible for this project. Open-air curing has been achieved by utilizing 365 nm light, which is encompassed in the peak absorption spectrum of the photoinitiator.

For the COMSOL model, the immediate next steps are to add the boundary fluxes from the air and support fluid. While this is a simple feature to add in COMSOL, finding the correct parameters for that feature requires further research since it involves analyzing and describing diffusion across fluid interfaces and determining values for the air, support fluid, and resin. While many oxygen concentrations and diffusion coefficients are known for many materials, finding values for conditions and materials that match the current setup is not trivial. This requires approximation, which is widely done, but approximation introduces variance into the model. A continuation of experimental data will be necessary for simulation validation. Other future COMSOL work involves accurately estimating chemical shrinkage. Once the model can accommodate chemical shrinkage, it will be possible to simulate the effect of various grayscale patterns through the model before implementing them experimentally, saving time and materials.

Future prototyping will seek to answer how the FISP system might be improved to increase the precision of layer thickness, print complex geometry, and reduce thermal shrinkage. Based on material properties and shrinkage, the desired light intensity must be determined for the 365nm light source. Then, steps need to be taken to automate the printing process. Automating the printing process and adding negative feedback control will allow the support fluid and resin layer heights to be more precisely and accurately controlled during a complete printing process. Using various geometries, simulated data accounting for mechanical shrinkage, should be compared to experimental data from the automated system. The comparison between the model and automated system will help to refine the model’s shrinkage. An accurate model is important to quickly analyze the effectiveness of grayscale masking techniques for reducing part shrinkage.

References

[1] N. Mulka, "Fluid Interface Supported Printing for Three-Dimensional Object Fabrication," Master's Thesis, George W. Woodruff School of Mechanical Engineering, Georgia Institute of Technology, Atlanta, GA, 2022.

[2] Ligon SC, Husár B, Wutzel H, Holman R, Liska R. Strategies to reduce oxygen inhibition in photoinduced polymerization. Chem Rev. 2014 Jan 8;114(1):557-89. doi: 10.1021/cr3005197. Epub 2013 Oct 1. PMID: 24083614.

[3] Wu, Xiangquan, et al. "Flexible Film Separation Analysis of LCD Based Mask Stereolithography." Journal of Materials Processing Technology, vol. 288, Feb. 2021, p. 116916. DOI.org (Crossref), https://doi.org/10.1016/j.jmatprotec.2020.116916.

[4] J. Wang, A. Jariwala, and D. Rosen, "Use of a Fluid Interface to Reduce Support Structures in Top-Down Stereolithography," 2022. doi: 10.26153/tsw/44223.

[5] M. Emami, and D. Rosen. An Improved Vat Photopolymerization Cure Model Demonstrates Photobleaching Effects. University of Texas at Austin, 2018. repositories.lib.utexas.edu, https://doi.org/10.26153/tsw/17195.

[6] Shenzen AnyCubic Technology, "UV Resin," CANEC1916332501, Aug. 2019.

[7] T. Scherzer and H. Langguth, "Temperature Dependence of the Oxygen Solubility in Acrylates and its Effect on the Induction Period in UV Photopolymerization," *Macromol. Chem. Phys.*, vol. 206, no. 2, pp. 240–245, 2005, doi: 10.1002/macp.200400300.

[8] K. Ruhland, *et al*, "Quantification and Elucidation of the UV-Light Triggered Initiation Kinetics of TPO and BPO in Liquid Acrylate Monomer", Journal of Applied Polymer Science, 2020, **137** (6), DOI: 10.1002/app.48357.

[9] G. W. Sluggett, et al, "(2,4,6-Trimethylbenzoyl)diphenylphosphine Oxide Photochemistry. A Direct Time-Resolved Spectroscopy Study of Both Radical Fragments," J. Amer. Chem. Soc., 1995, 117, 5148-5153.

[10] S. Jockusch, et al, "A Steady-State and Picosecond Pump-Probe Investigation of an Acyl and a Bis(acyl)phosphine Oxide", J. Amer. Chem. Soc., 1997, 119, 11495-11501.

[11] C. Dietlin, et al, "Rational Design of Acyldiphenylphosphine Oxides as Photoinitiators of Radical Polymerization", Macromolecules, 2019, 52 (20), 7886-7893.